Advances in Computational Design, *Vol. 10, No. 3 (2025) 251-273*
https://doi.org/10.12989/acd.2025.10.3.251

Sinusoidal shear deformation theory for dynamic analysis of FG plates under various boundary conditions: Influence of micromechanical models

Mohamed Saad[1], Latifa Ould Larbi[2], Lazreg Hadji[3], Nafissa Zouatnia*[3], Hassen Ait Atmane[2] and Royal Madan[4]

[1]*Department of Mechanical Engineering, University of Tiaret, BP 78 Zaaroura, 14000 Tiaret, Algeria*
[2]*Laboratory of Structures, Geotechnics and Risks, Department of Civil Engineering, Hassiba Benbouali University of Chlef, Chlef, Algeria*
[3]*Department of Civil Engineering, University of Tiaret, BP 78 Zaaroura, 14000 Tiaret, Algeria*
[4]*Department of Mechanical Engineering, Graphic Era (Deemed to be University) Dehradun- 248002, Uttarakhand, India*

(Received June 5, 2025, Revised July 22, 2025, Accepted July 25, 2025)

Abstract. In the present study, free vibration analysis of an FG plate has been performed by employing trigonometric shear deformation plate theory. The selection of an appropriate homogenization model is important as it could significantly influence the material behavior. Therefore, well-known micromechanical models such as Voigt, Reuss, and representative volume element method have been studied and their results are compared. The effect of various boundary conditions was also seen by changing the boundary conditions as SSSS, CCCC, CSCS, and FCFC. The mechanical properties change uni-directionally across the thickness according to a simple power law. Hamilton's principle is applied to derive the governing equations of motion, and Navier-type analytical solutions are formulated for vibration analysis. The study examined the impact of the power-law index, length-to-thickness ratio, micromechanical models, and boundary conditions on the natural frequencies of the FG plate.

Keywords: boundary conditions; FG plate; free vibration; functionally graded material; micromechanical models

1. Introduction

Functionally graded materials (FGMs) are special composites in which the material properties change along specific directions. The changes in the properties arise because of a change in composition, microstructure, or porosity Almasi *et al*. (2016). Usually, the fabrication involves the mixing of two or more materials to obtain functional requirements. Additionally, based on the application, the gradation variation can be unidirectional, bidirectional, or multidirectional Hadji *et al*. (2024). This smooth transition in material properties can be customized to meet the requirements of various industries and engineering applications (Bakar *et al*. 2018, Birman and

*Corresponding author, Ph.D., E-mail: nafissa.zouatnia@univ-tiaret.dz

http://www.techno-press.org/?journal=acd&subpage=7 ISSN: 2383-8477 (Print), 2466-0523 (Online)

Kardomateas 2018, Ermakova *et al*. 2019). FGMs provide a gradual variation in microstructure, reducing property mismatches across the interface (Suresh and Mortensen, 1997). Bending analysis of FG rotating disks under different boundary conditions was carried out using a semi-analytical solution. They found that stress induced in an FG disk was lower compared to disks made up of isotropic material (full-metal and full-ceramics) were higher than stresses induced in an FG disk Bayat *et al*. (2008). Presented an analytical solution of sound transmission loss corrugated core FGM plates filled with a porous material, wherein two modes of FGM sandwich plates were considered, which contain one with homogeneous face sheets, metal or ceramic, and FGM core, and the other with FGM face sheets and homogeneous metal or ceramic core Wang *et al*. (2024).

A 3D vibration analysis of layered FG cylindrical sandwich shells was performed analytically Arefi *et al*. (2018). The most important result they obtained was that the frequency decreases when the index of non-homogeneous (FGP) layers increases, while the frequency rises significantly when the ratio of the thickness of the middle layer to the length of the cylinder increases. A first-order shear deformation theory was used to study the behavior of vibration of FGM truncated conical shells surrounded by Winkler and Pasternak foundation. The shear strains lead to a reduction of the value of the frequency parameters from 2.71% to 0.58%. The dynamic stability of a functionally graded orthotropic cylindrical shell resting on an elastic foundation under a linearly increasing load, with the influence of damping, was investigated by Gao *et al*. (2018). Further, the third-order shear deformation theory is used to analyze the free vibration of a 2D-FGM beam under different boundary conditions Karamanlı, (2018). They found that increasing the gradient index in the direction of the thickness leads to a reduction in natural frequencies of clamped-clamped 2D-FGB. Investigated free and forced vibrations of both FG and homogeneous thick plates by employing the meshless local Petrov-Galerkin approach with higher-order and normal deformable shear deformation plate theory Qian *et al*. (2003).

Vibration and buckling analysis were performed on a circular cylindrical shell using higher-order shear deformation theory and Hamilton's principle Lang and Xuewu (2013). The free vibration of stiffened FGM cylindrical shells resting on the Pasternak elastic foundation using a semi-analytical finite strip approach with various shell theories was performed Kim (2015). The porosity influence on the free vibration of FGM nanoplates resting on a Winkler and Pasternak foundation was studied Mechab *et al*. (2016). Examined free vibrations of porous FGM rectangular plates under uniform elastic boundary conditions by applying an improved Fourier series approach Zhao *et al*. (2019). The nonlinear vibration response of functionally graded thick plates under thermal stress, supported by an elastic foundation, was analyzed using the third-order shear deformation plate theory Duc *et al*. (2016), which found that the foundation helps reduce vibration amplitude in a thermal environment. The vibration response of sandwich structures under varying boundary conditions, and geometrical and material parameters with and without porosity effects, was performed analytically (Hadji *et al*. 2019, Zouatnia *et al*. 2024).

Dynamic analysis of homogeneous FG thick plates was performed using the meshless local Petrov-Galerkin approach with higher-order and normal deformable shear deformation plate theory Qian *et al*. (2003). In another study, von-Karman non-linearity and Kriging interpolation were employed to study the free vibration of FG circular plates under a thermal environment Zhu and Liew (2012). Free and forced vibration of FG thin circular plates in terms of von Karman's nonlinear dynamic equations with the Kantorovich time averaging method was performed Alibeigloo and Liew (2014). An axisymmetric bending of two-directional functionally graded circular and annular plates with material properties varying exponentially in thickness and radial

directions was performed using a semi-analytical method. The method shows high accuracy and computational efficiency compared to the finite element method Nie and Zhong (2007). A dynamic stiffness matrix method for vibration analysis of porous power-law functionally graded Levy-type plates was performed using Kirchhoff-Love plate theory and Hamilton's principle. The effect of various parameters on eigenvalues demonstrates high accuracy and computational efficiency Ali and Azam (2021). The dynamic analysis of the FG plate has been thoroughly examined under different loading conditions using methods like simple quasi-3D hyperbolic theory Addou *et al*. (2019), integral refined plate theory (Balubaid *et al*. 2019) high-order shear deformation plate theory (Ding *et al*. 2023), a radial basis function-based meshless collocation Srivastava *et al*. (2025), First shear deformation theory (Bendenia *et al*. 2020). Hamilton's principle along with the extended Kantorovich method for laminated panels, was employed and solved numerically Singh and Kumari (2020), a modified bulge test with FEM for MEMS diaphragms Altabey (2017), Higher-order shear deformation theory with Monte Carlo simulations for functionally graded plates (Achchhe *et al*. (2017). To analyze nonlocal thermoelastic nanobeams a Laplace transformation method was utilized Zenkour and Abouelregal (2018), while a semi-analytical approach is used to study magneto-thermo-elastic effects in piezoelectric hollow spheres by Allam *et al*. (2018). These findings offer valuable insights into material behavior under complex conditions, contributing to advancements in engineering design and analysis.

Recently, many articles have been published on the subject of vibration of FGM structures. For exaples, Hadji *et al*. (2019) used an analytical solution for bending and free vibration responses of functionally graded beams with porosities: Effect of the micromechanical models. Djebbour *et al*. (2024) used an enhanced quasi-3D HSDT for free vibration analysis of porous FG-CNT beams on a new concept of orthotropic VE-foundations. Nebab *et al*. (2024) investigated the fundamental frequencies of cracked FGM beams with influence of porosity and Winkler/Pasternak/Kerr foundation support using a new quasi-3D HSDT. Hadji *et al*. (2025) developed dynamic behavior of imperfect FGM beams with various porosity distribution rates: analysis and modeling. Lakal *et al*. (2024) investigated the natural frequency analysis of FG-GNPR nanoplates under different boundary conditions. Ghazwani *et al*. (2024) examinated the high-frequency behavior of functionally graded porous nanobeams using nonlocal simple higher-order shear deformation theory. Alnujaie *et al*. (2025) studied Damped vibration characteristics of functionally graded sandwich beams resting on an advanced viscoelastic foundation model.

The mechanical properties of composites/ FGMs can be estimated analytically or numerically. Analytically, there are well-known methods like the Voigt model Voigt (1889), the Reuss model Reuss (1929), and the Mori-Tanaka model Affdl and Kardos (1976) to name a few. The rule of mixture, the Voigt and Reuss models yield the upper and lower bounds because they assume that the binding between the phases (fiber and matrix) is perfect. Therefore, these models can be utilized to test newly developed models because all the developed model results must fall between these two bounds. However, literature reveals that these models are not effective when the reinforcement is of a particulate type (Madan and Bhowmick, 2021). Therefore, a modified rule of mixture was proposed, which consists of an empirical parameter, a stress-strain transfer ratio Nakamura *et al*. (2000). Later, the value of this parameter was identified for the Al-SiC composite Kapuria *et al*. (2008). They found that the parameter does not vary much with the composition change, and hence, a constant value can be considered for analysis purposes Madan *et al*. (2020). As the parameter is different for different materials so investigating the parameter experimentally for several composite combinations is not feasible as it incurs a huge cost and time. Therefore, other analytical approaches have been identified to identify the parameters for a combination of

metal-ceramic, metal-metal, and ceramic-ceramic materials. In one such study, an RVE-based technique to estimate the mechanical properties of a hybrid composite is proposed. The study was first validated for two-phase composites, which was later extended to three-phase composites Madan *et al*. (2025).

This study aims to develop a trigonometric shear deformation plate theory for analyzing the free vibration behavior of functionally graded (FG) plates. The key innovation of this theory lies in the introduction of a novel shear strain shape function, which ensures a realistic distribution of transverse shear strains through the plate thickness. Additionally, it naturally satisfies the tangential stress-free boundary conditions on the plate surface without requiring a shear correction factor. The free vibration problem for the FG plate was solved for various micromechanical models. A continuous power law variation of the material property was considered along the thickness. The equations of motion of FG plates are obtained from Hamilton's principle and solved via Navier's procedure. Analytical solutions for free vibration are obtained. To validate the efficacy of the proposed theory, the study conducts numerous numerical validations that explore the influence of various geometrical parameters, boundary conditions, and grading indices. Moreover, the analysis was extended for different boundary conditions that have not been explored before. The effects of various variables, such as span-to-depth ratio, gradient index, boundary conditions, and micromechanical models on the free vibration of FG plates are all discussed. The study thus provides valuable guidance to design engineers in selecting the desired geometry and material parameters for different engineering applications.

2. Effective properties of FGMs

FGMs differ from conventional microstructures due to their spatially varying material properties, making micromechanical modeling more complex Yu and Kidane (2014). Several micromechanics models have been developed to determine the effective properties of FGMs. The following section outlines some of these models for determining the effective properties of an FG plate.

2.1 Voigt model

The Voigt model, originally proposed by Voigt (1889), is based on the assumption of uniform strain across all constituent phases (iso-strain condition), implying that all phases undergo the same deformation. Under this model, the following assumptions are made:

- ✓ Uniform strain distribution across all phases
- ✓ Perfect interfacial bonding between the matrix and the reinforcement
- ✓ The model yields an upper bound estimate for the effective stiffness (Young's modulus) of the composite.

$$E(z) = E_c V_c + E_m(1 - V_c) \tag{1}$$

2.2 Reuss model

The Reuss model, proposed by Reuss (1929), assumes uniform stress across all constituent phases (iso-stress condition), which results in different strains in each phase. Under this model, the

following assumptions are made:

- ✓ Uniform stress distribution across all phases
- ✓ Perfect bonding between the matrix and the reinforcement
- ✓ The model provides a lower bound estimate for the effective stiffness (Young's modulus) of the composite.

$$E(z) = \frac{E_c E_m}{E_c(1 - V_c) + E_m V_c} \tag{2}$$

2.3 Tamura model

The Tamura model applies a linear rule of mixtures and incorporates an empirical fitting parameter called the stress-to-strain transfer(q) Benveniste, (1987), with the present assumptions:

- ✓ Linear rule of mixtures with an empirical parameter q (stress-to-strain transfer ratio).
- ✓ q = 0 reduces to the Reuss model, q→∞ reduces to the Voigt model.
- ✓ Requires experimental calibration for q.

The Tamura model (Benveniste 1987) extends the linear rule of mixtures by introducing an empirical fitting parameter, q, referred to as the stress-to-strain transfer ratio. Its underlying premises are as follows:

- ✓ A linear rule of mixtures augmented by the parameter q.
- ✓ When q = 0, the model degenerates to the Reuss lower bound approximation, whereas q→∞ recovers the Voigt upper-bound limit.
- ✓ The value of q must be calibrated experimentally for each composite system.

$$q = \frac{\sigma_1 - \sigma_2}{\varepsilon_1 - \varepsilon_2} \tag{3}$$

Where when $q = 0$ correspond to the Reuss rule while $q = 100$ gives the Voigt rule. The parameter (q) can only be computed experimentally, which restricts its employability in estimating material properties effectively. Later, in one of the studies, the authors identified an alternative to estimate $\boldsymbol{q}$ numerically. The effective Young's modulus is found as

$$E(z) = \frac{(1 - V_c)E_m(q - E_c) + V_c E_c(q - E_m)}{(1 - V_c)(q - E_c) + V_c E_c(q - E_m)} \tag{4}$$

2.4 Description by a representative volume element (LRVE)

The Local Representative Volume Element (LRVE) is defined at the mesoscopic scale—significantly larger than the characteristic length of individual particles (inhomogeneities), yet smaller than the overall dimensions of the macroscopic specimen (Blanco *et al*. 2016). This approach is formulated under the assumption that the microstructure of the heterogeneous material is known. Within the deterministic micromechanical framework, the LRVE commonly employs volume or ensemble averages of microstructural descriptors as input.

Using the LRVE approach, Young's modulus can be determined as described by Akbarzadeh *et al*. (2015), based on the following assumptions:

- ✓ The microstructure is statistically homogeneous at the mesoscale,
- ✓ Volume averaging is applicable for homogenization,

✓ The size of the LRVE is much greater than that of the inhomogeneities but smaller than the macroscopic specimen.

$$E(z) = E_m\left(1 + \frac{V_c}{FE - \sqrt[3]{V_c}}\right), \qquad FE = \frac{1}{1 - \frac{E_m}{E_c}} \tag{5}$$

2.5 Mori-Tanaka model

Micromechanical models, such as the Mori–Tanaka scheme, are commonly employed to estimate the locally effective material properties of composite systems. This approach considers a two-phase composite comprising a matrix reinforced with randomly distributed spherical inclusions. Based on the previously outlined assumptions, Young's modulus can be derived under the following conditions:

✓ Spherical inclusions are randomly dispersed within the matrix

✓ A dilute concentration of inclusions is assumed, allowing the use of Eshelby's solution to account for interaction effects

The effective elastic properties are influenced by the volume fraction and geometric characteristics (e.g., shape) of the inclusions

$$E(z) = E_m + (E_c - E_m)\left(\frac{V_c}{1 + (1 - V_c)(E_c/E_m - 1)(1 + \nu)/(3 - 3\nu)}\right) \tag{6}$$

where $V_c = \left(\frac{1}{2} + \frac{z}{h}\right)^p$ is the volume fraction of the ceramic and where p is the power law index. Since the effects of the variation of Poisson's ratio (ν) on the response of FGM plates are very small Kitipornchai *et al*. (2006), this material parameter is assumed to be constant for convenience.

3. Mathematical modeling

3.1 Functionally graded plates

Considered an FG plate made up of metal-ceramic phases, as shown in Fig.1. The variation of material properties through the plate's thickness is modeled using a power-law distribution, as described by Eq. (7) (Thai and Choi 2014). This formulation is based on the following assumptions:

Material properties vary smoothly and continuously through the thickness of the plate

Poisson's ratio is assumed to remain constant, as its variation is considered negligible

$$P(z) = (P_t - P_b)\left(\frac{z}{h} + \frac{1}{2}\right)^p + P_b \tag{7}$$

where P_t and P_b denote values of the material properties at the top and bottom of the plate, respectively, and p is the power-law index. According to this distribution, the bottom surface $(z = -h/2)$ of the functionally graded plate is pure metal, whereas the top surface $(z = h/2)$ is pure ceramics, and for different values of k, one can obtain different volume fractions of metal.

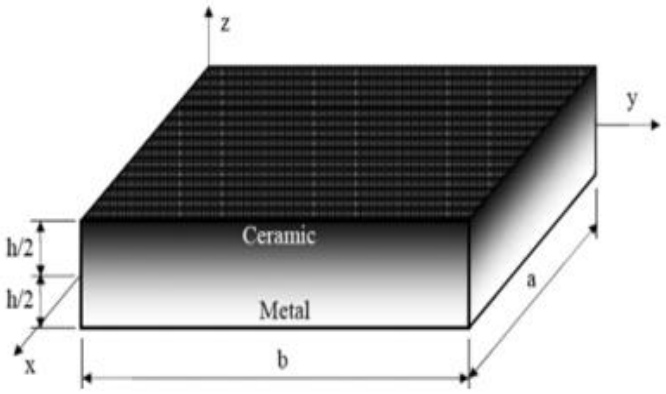

Fig. 1 Geometry of Rectangular FG Plate and Coordinates

3.2 Kinematic, strain and stress relations

The displacement fields can be defined by Touratier (1991):

$$\begin{aligned} U(x,y,z,t) &= u_0(x,y,t) - z\frac{\partial w_b}{\partial x} - f(z)\frac{\partial w_s}{\partial x} \\ V(x,y,z,t) &= v_0(x,y,t) - z\frac{\partial w_b}{\partial y} - f(z)\frac{\partial w_s}{\partial y} \\ W(x,y,z,t) &= w_b(x,y,t) + w_s(x,y,t) \end{aligned} \tag{8}$$

In which t represents the time, u_0 and v_0 signify the displacement functions of the middle surfaces of the plate. Also, $f(z)$ refers to the variation of the transverse shear strain along with the plate thickness. In this study, we use a sinusoidal-type shape function given by (Touratier 1991).

$$f(z) = z - \frac{h}{\pi} sin\left(\frac{\pi z}{h}\right) \tag{9}$$

It is worth mentioning that by considering $f(z)$=0 and $f(z)$=z, the presented theory will reduce to CPT and FSDT, respectively.

The nonzero strains associated with the displacement field in Eq. (8) are:

$$\begin{Bmatrix} \varepsilon_x \\ \varepsilon_y \\ \gamma_{xy} \end{Bmatrix} = \begin{Bmatrix} \varepsilon_x^0 \\ \varepsilon_y^0 \\ \gamma_{xy}^0 \end{Bmatrix} + z\begin{Bmatrix} k_x^b \\ k_y^b \\ k_{xy}^b \end{Bmatrix} + f(z)\begin{Bmatrix} k_x^s \\ k_y^s \\ k_{xy}^s \end{Bmatrix}, \quad \begin{Bmatrix} \gamma_{yz} \\ \gamma_{xz} \end{Bmatrix} = g(z)\begin{Bmatrix} \gamma_{yz}^s \\ \gamma_{xz}^s \end{Bmatrix} \tag{10}$$

where

$$\begin{Bmatrix} \varepsilon_x^0 \\ \varepsilon_y^0 \\ \gamma_{xy}^0 \end{Bmatrix} = \begin{Bmatrix} \frac{\partial u_0}{\partial x} \\ \frac{\partial v_0}{\partial x} \\ \frac{\partial u_0}{\partial y} + \frac{\partial v_0}{\partial x} \end{Bmatrix}, \quad \begin{Bmatrix} k_x^b \\ k_y^b \\ k_{xy}^b \end{Bmatrix} = \begin{Bmatrix} -\frac{\partial^2 w_b}{\partial x^2} \\ -\frac{\partial^2 w_b}{\partial y^2} \\ -2\frac{\partial^2 w_b}{\partial x \partial y} \end{Bmatrix}, \quad \begin{Bmatrix} k_x^s \\ k_y^s \\ k_{xy}^s \end{Bmatrix} = \begin{Bmatrix} -\frac{\partial^2 w_s}{\partial x^2} \\ -\frac{\partial^2 w_s}{\partial y^2} \\ -2\frac{\partial^2 w_s}{\partial x \partial y} \end{Bmatrix}, \quad \begin{Bmatrix} \gamma_{yz}^s \\ \gamma_{xz}^s \end{Bmatrix} = \begin{Bmatrix} \frac{\partial w_s}{\partial y} \\ \frac{\partial w_s}{\partial x} \end{Bmatrix} \tag{11a}$$

$$g(z) = 1 - \frac{df(z)}{dz} \tag{11b}$$

The linear constitutive relations of an FG plate can be written as

$$\begin{Bmatrix} \sigma_x \\ \sigma_y \\ \tau_{xy} \end{Bmatrix} = \begin{bmatrix} C_{11} & C_{12} & 0 \\ C_{12} & C_{22} & 0 \\ 0 & 0 & C_{66} \end{bmatrix} \begin{Bmatrix} \varepsilon_x \\ \varepsilon_y \\ \gamma_{xy} \end{Bmatrix} \tag{12a}$$

$$\begin{Bmatrix} \tau_{yz} \\ \tau_{zx} \end{Bmatrix} = \begin{bmatrix} C_{44} & 0 \\ 0 & C_{55} \end{bmatrix} \begin{Bmatrix} \gamma_{yz} \\ \gamma_{zx} \end{Bmatrix} \tag{12b}$$

in which,

$$\begin{aligned} C_{11} &= C_{22} = \frac{E(z)}{1-\nu^2} \\ C_{12} &= \frac{\nu\, E(z)}{1-\nu^2} \\ C_{44} &= C_{55} = C_{66} = \frac{E(z)}{2(1+\nu)} \end{aligned} \tag{13}$$

3.3 Equations of motion

Hamilton's principle is employed to derive the equations of motion, following the formulation presented by Reddy (2002). The application of this principle is based on the following assumptions:

- ✓ The system is conservative, with no energy dissipation
- ✓ The principle of virtual work is applicable, assuming small deformations

$$0 = \int_0^t (\delta\, U - \delta\, K)\, dt \tag{11b}$$

where $\delta\, U$ is the variation of strain energy, and $\delta\, K$ is the variation of kinetic energy. The variation of strain energy of the plate is given by

$$\begin{aligned} \delta\, U &= \int_V \left[\sigma_x \delta\, \varepsilon_x + \sigma_y \delta\, \varepsilon_y + \tau_{xy} \delta\, \gamma_{xy} + \tau_{yz} \delta\, \gamma_{yz} + \tau_{xz} \delta\, \gamma_{xz}\right] dV \\ &= \int_A \left[N_x \delta\, \varepsilon_x^0 + N_y \delta\, \varepsilon_y^0 + N_{xy} \delta\, \gamma_{xy}^0 + M_x^b \delta\, k_x^b + M_y^b \delta\, k_y^b + M_{xy}^b \delta\, k_{xy}^b \right. \\ &\quad \left. + M_x^s \delta\, k_x^s + M_y^s \delta\, k_y^s + M_{xy}^s \delta\, k_{xy}^s + S_{yz}^s \delta\, \gamma_{yz}^s + S_{xz}^s \delta\, \gamma_{xz}^s\right] dA = 0 \end{aligned} \tag{15}$$

where A is the top surface and the stress resultants N, M, and S are defined by

$$\left(N_i, M_i^b, M_i^s\right) = \int_{-h/2}^{h/2} (1, z, f)\sigma_i dz \;\; (i = x, y, xy) \tag{16a}$$

$$\left(S_{xz}^s, S_{yz}^s\right) = \int_{-h/2}^{h/2} g\left(\tau_{xz}, \tau_{yz}\right) dz \tag{16b}$$

Variation of the kinetic energy of the plate can be expressed as

$$\begin{aligned}
\delta K &= \int_{-\frac{h}{2}}^{\frac{h}{2}}\int_A [\dot{u}\delta\dot{u} + \dot{v}\delta\dot{v} + \dot{w}\delta\dot{w}]\,\rho(z)\,dA\,dz \\
&= \int_A \{I_0[\dot{u}_0\delta\dot{u}_0 + \dot{v}_0\delta\dot{v}_0 + (\dot{w}_b+\dot{w}_s)(\delta\dot{w}_b+\delta\dot{w}_s)] \\
&-I_1\left(\dot{u}_0\frac{\partial\delta\dot{w}_b}{\partial x} + \frac{\partial\dot{w}_b}{\partial x}\delta\dot{u}_0 + \dot{v}_0\frac{\partial\delta\dot{w}_b}{\partial y} + \frac{\partial\dot{w}_b}{\partial y}\delta\dot{v}_0\right) \\
&-I_2\left(\dot{u}_0\frac{\partial\delta\dot{w}_s}{\partial x} + \frac{\partial\dot{w}_s}{\partial x}\delta\dot{u}_0 + \dot{v}_0\frac{\partial\delta\dot{w}_s}{\partial y} + \frac{\partial\dot{w}_s}{\partial y}\delta\dot{v}_0\right) \\
&+J_1\left(\frac{\partial\dot{w}_b}{\partial x}\frac{\partial\delta\dot{w}_b}{\partial x} + \frac{\partial\dot{w}_b}{\partial y}\frac{\partial\delta\dot{w}_b}{\partial y}\right) + K_2\left(\frac{\partial\dot{w}_s}{\partial x}\frac{\partial\delta\dot{w}_s}{\partial x} + \frac{\partial\dot{w}_s}{\partial y}\frac{\partial\delta\dot{w}_s}{\partial y}\right) \\
&+J_2\left(\frac{\partial\dot{w}_b}{\partial x}\frac{\partial\delta\dot{w}_s}{\partial x} + \frac{\partial\dot{w}_s}{\partial x}\frac{\partial\delta\dot{w}_b}{\partial x} + \frac{\partial\dot{w}_b}{\partial y}\frac{\partial\delta\dot{w}_s}{\partial y} + \frac{\partial\dot{w}_s}{\partial y}\frac{\partial\delta\dot{w}_b}{\partial y}\right)\Big\}dA
\end{aligned} \tag{17}$$

in which dot-superscript convention indicates the differentiation with respect to the time t, $\rho(z)$ is the mass density given by Eq. (7), and $(I_i,\ J_i, K_i)$ are mass inertias expressed by

$$(I_0, I_1, I_2) = \int_{-h/2}^{h/2}(1, z, z^2)\rho(z)dz \tag{18a}$$

$$(J_1, J_2, K_2) = \int_{-h/2}^{h/2}(f, z\,f, f^2)\rho(z)dz \tag{18b}$$

By substituting Eqs. (15) and (17) into Eq. (14), the following can be derived:

$$\begin{aligned}
&\delta u_0\colon\ \frac{\partial N_x}{\partial x} + \frac{\partial N_{xy}}{\partial y} = I_0\ddot{u}_0 - I_1\frac{\partial\ddot{w}_b}{\partial x} - J_1\frac{\partial\ddot{w}_s}{\partial x} \\
&\delta v_0\colon\ \frac{\partial N_{xy}}{\partial x} + \frac{\partial N_y}{\partial y} = I_0\ddot{v}_0 - I_1\frac{\partial\ddot{w}_b}{\partial y} - J_1\frac{\partial\ddot{w}_s}{\partial y} \\
&\delta w_b\colon\ \frac{\partial^2 M_x^b}{\partial x^2} + 2\frac{\partial^2 M_{xy}^b}{\partial x\partial y} + \frac{\partial^2 M_y^b}{\partial y^2} = I_0(\ddot{w}_b+\ddot{w}_s) + I_1\left(\frac{\partial\ddot{u}_0}{\partial x} + \frac{\partial\ddot{v}_0}{\partial y}\right) - I_2\nabla^2\ddot{w}_b - J_2\nabla^2\ddot{w}_s \\
&\delta w_s\colon\ \frac{\partial^2 M_x^s}{\partial x^2} + 2\frac{\partial^2 M_{xy}^s}{\partial x\partial y} + \frac{\partial^2 M_y^s}{\partial y^2} + \frac{\partial S_{xz}^s}{\partial x} + \frac{\partial S_{yz}^s}{\partial y} \\
&= I_0(\ddot{w}_b+\ddot{w}_s) + J_1\left(\frac{\partial\ddot{u}_0}{\partial x} + \frac{\partial\ddot{v}_0}{\partial y}\right) - J_2\nabla^2\ddot{w}_b - K_2\nabla^2\ddot{w}_s
\end{aligned} \tag{19}$$

Substituting Eq. (10) into Eq. (12) and the subsequent results into Eqs. (16), the stress resultants are obtained in terms of strains as following compact form:

$$\begin{Bmatrix} N \\ M^b \\ M^s \end{Bmatrix} = \begin{bmatrix} A & B & B^s \\ B & D & D^s \\ B^s & D^s & H^s \end{bmatrix}\begin{Bmatrix} \varepsilon \\ k^b \\ k^s \end{Bmatrix}, \quad S = A^s\gamma \tag{20}$$

in which

$$N = \{N_x, N_y, N_{xy}\}^t,\ M^b = \{M_x^b, M_y^b, M_{xy}^b\}^t, \quad M^s = \{M_x^s, M_y^s, M_{xy}^s\}^t \tag{21a}$$

$$\varepsilon = \left\{\varepsilon_x^0, \varepsilon_y^0, \gamma_{xy}^0\right\}^t, \quad k^b = \left\{k_x^b, k_y^b, k_{xy}^b\right\}^t, \quad k^s = \left\{k_x^s, k_y^s, k_{xy}^s\right\}^t \tag{21b}$$

$$A = \begin{bmatrix} A_{11} & A_{12} & 0 \\ A_{12} & A_{22} & 0 \\ 0 & 0 & A_{66} \end{bmatrix}, \quad B = \begin{bmatrix} B_{11} & B_{12} & 0 \\ B_{12} & B_{22} & 0 \\ 0 & 0 & B_{66} \end{bmatrix}, \quad D = \begin{bmatrix} D_{11} & D_{12} & 0 \\ D_{12} & D_{22} & 0 \\ 0 & 0 & D_{66} \end{bmatrix} \tag{21c}$$

$$B^s = \begin{bmatrix} B_{11}^s & B_{12}^s & 0 \\ B_{12}^s & B_{22}^s & 0 \\ 0 & 0 & B_{66}^s \end{bmatrix}, D^s = \begin{bmatrix} D_{11}^s & D_{12}^s & 0 \\ D_{12}^s & D_{22}^s & 0 \\ 0 & 0 & D_{66}^s \end{bmatrix}, \quad H^s = \begin{bmatrix} H_{11}^s & H_{12}^s & 0 \\ H_{12}^s & H_{22}^s & 0 \\ 0 & 0 & H_{66}^s \end{bmatrix} \tag{21d}$$

$$S = \left\{S_{xz}^s, S_{yz}^s\right\}^t, \quad \gamma = \left\{\gamma_{xz}^s, \gamma_{yz}^s\right\}^t, \quad A^s = \begin{bmatrix} A_{44}^s & 0 \\ 0 & A_{55}^s \end{bmatrix} \tag{21e}$$

and stiffness components are given as:

$$\begin{Bmatrix} A_{11} & B_{11} & D_{11} & B_{11}^s & D_{11}^s & H_{11}^s \\ A_{12} & B_{12} & D_{12} & B_{12}^s & D_{12}^s & H_{12}^s \\ A_{66} & B_{66} & D_{66} & B_{66}^s & D_{66}^s & H_{66}^s \end{Bmatrix} = \int_{-h/2}^{h/2} C_{11}(1, z, z^2, f(z), z\,f(z), f^2(z)) \begin{Bmatrix} 1 \\ \nu \\ \dfrac{1-\nu}{2} \end{Bmatrix} dz \tag{22}$$

with

$$(A_{22}, B_{22}, D_{22}, B_{22}^s, D_{22}^s, H_{22}^s) = (A_{11}, B_{11}, D_{11}, B_{11}^s, D_{11}^s, H_{11}^s) \tag{23a}$$

$$A_{44}^s = A_{55}^s = \int_{-h/2}^{h/2} C_{44}[g(z)]^2 dz \tag{23b}$$

Introducing Eq. (20) into Eq. (21), the equations of motion can be expressed in terms of displacements ($u_0,\ v_0,\ w_b,\ w_s$) and the appropriate equations take the form:

$$\begin{aligned} &A_{11}\frac{\partial^2 u_0}{\partial x^2} + A_{66}\frac{\partial^2 u_0}{\partial y^2} + (A_{12}+A_{66})\frac{\partial^2 v_0}{\partial x \partial y} - B_{11}\frac{\partial^3 w_b}{\partial x^3} - (B_{12}+2B_{66})\frac{\partial^3 w_b}{\partial x \partial y^2} \\ &-B_{11}^s\frac{\partial^3 w_s}{\partial x^3} - (B_{12}^s+2B_{66}^s)\frac{\partial^3 w_s}{\partial x \partial y^2} = I_0\ddot{u}_0 - I_1\frac{\partial \ddot{w}_b}{\partial x} - J_1\frac{\partial \ddot{w}_s}{\partial x} \end{aligned} \tag{24a}$$

$$\begin{aligned} &(A_{12}+A_{66})\frac{\partial^2 u_0}{\partial x \partial y} + A_{66}\frac{\partial^2 v_0}{\partial x^2} + A_{22}\frac{\partial^2 v_0}{\partial y^2} - (B_{12}+2B_{66})\frac{\partial^3 w_b}{\partial x^2 \partial y} - B_{22}\frac{\partial^3 w_b}{\partial y^3} \\ &-B_{22}^s\frac{\partial^3 w_s}{\partial y^3} - (B_{12}^s+2B_{66}^s)\frac{\partial^3 w_s}{\partial x^2 \partial y} = I_0\ddot{v}_0 - I_1\frac{\partial \ddot{w}_b}{\partial y} - J_1\frac{\partial \ddot{w}_s}{\partial y} \end{aligned} \tag{24b}$$

$$\begin{aligned} &B_{11}\frac{\partial^3 u_0}{\partial x^3} + (B_{12}+2B_{66})\frac{\partial^3 u_0}{\partial x \partial y^2} + (B_{12}+2B_{66})\frac{\partial^3 v_0}{\partial x^2 \partial y} + B_{22}\frac{\partial^3 v_0}{\partial y^3} - D_{11}\frac{\partial^4 w_b}{\partial x^4} \\ &-2(D_{12}+2D_{66})\frac{\partial^4 w_b}{\partial x^2 \partial y^2} - D_{22}\frac{\partial^4 w_b}{\partial y^4} - D_{11}^s\frac{\partial^4 w_s}{\partial x^4} - 2(D_{12}^s+2D_{66}^s)\frac{\partial^4 w_s}{\partial x^2 \partial y^2} \\ &-D_{22}^s\frac{\partial^4 w_s}{\partial y^4} = I_0(\ddot{w}_b+\ddot{w}_s) + I_1\left(\frac{\partial \ddot{u}_0}{\partial x} + \frac{\partial \ddot{v}_0}{\partial y}\right) - I_2\nabla^2\ddot{w}_b - J_2\nabla^2\ddot{w}_s, \end{aligned} \tag{24c}$$

$$B_{11}^s\frac{\partial^3 u}{\partial x^3} + (B_{12}^s+2B_{66}^s)\frac{\partial^3 u}{\partial x \partial y^2} + (B_{12}^s+2B_{66}^s)\frac{\partial^3 v}{\partial x^2 \partial y} + B_{22}^s\frac{\partial^3 v}{\partial y^3} - D_{11}^s\frac{\partial^4 w_b}{\partial x^4} \tag{24d}$$

$$-2(D_{12}^s+2D_{66}^s)\frac{\partial^4 w_b}{\partial x^2\partial y^2}-D_{22}^s\frac{\partial^4 w_b}{\partial y^4}-H_{11}^s\frac{\partial^4 w_s}{\partial x^4}-2(H_{12}^s+2H_{66}^s)\frac{\partial^4 w_s}{\partial x^2\partial y^2}-H_{22}^s\frac{\partial^4 w_s}{\partial y^4}$$
$$+A_{55}^s\frac{\partial^2 w_s}{\partial x^2}+A_{44}^s\frac{\partial^2 w_s}{\partial y^2}=I_0(\ddot{w}_b+\ddot{w}_s)+J_1\left(\frac{\partial\ddot{u}_0}{\partial x}+\frac{\partial\ddot{v}_0}{\partial y}\right)-J_2\nabla^2\ddot{w}_b-K_2\nabla^2\ddot{w}_s$$

3.4 Solution method

In this section, an exact solution for the free vibration analysis of FG plates i.e., Eqs. (24) is presented. The boundary conditions for an arbitrary edge with simply supported and clamped conditions are:

- Clamped (C)

$$u_0=v_0=w_b=\partial w_b/\partial x=\partial w_b/\partial y=w_s=\partial w_s/\partial x=\partial w_s/\partial y \quad \text{at} \quad x=0,a \text{and} \ y=0,b \tag{25a}$$

- Simply supported (S)

$$v_0=w_b=\partial w_b/\partial y=w_s=\partial w_s/\partial y=0 \ \text{ at } \ x=0,a \tag{26a}$$

$$u_0=w_b=\partial w_b/\partial x=w_s=\partial w_s/\partial x=0 \ \text{ at } \quad y=0,b \tag{26b}$$

The following representation for the displacement quantities that satisfy the above boundary conditions, is appropriate in the case of this problem

$$\begin{Bmatrix}u_0\\v_0\\w_b\\w_s\end{Bmatrix}=\begin{Bmatrix}U_{mn}\dfrac{\partial X_m(x)}{\partial x}Y_n(y)e^{i\omega t}\\V_{mn}X_n(x)\dfrac{\partial Y_n(y)}{\partial y}e^{i\omega t}\\W_{bmn}X_n(x)Y_n(y)e^{i\omega t}\\W_{smn}X_n(x)Y_n(y)e^{i\omega t}\end{Bmatrix} \tag{27}$$

where U_{mn}, V_{mn}, W_{bmn}, and W_{smn} are arbitrary parameters and $\omega=\omega_{mn}$ denotes the eigenfrequency associated with $(m,n)^{th}$eigenmode. The functions $X_m(x)$ and $Y_n(y)$ represent approximate shapes of the deflected surface of the plate which should satisfy geometric boundary conditions given in Eqs. (25) and (26). For the different cases of boundary conditions, these functions are listed in Table 1 noting that $\lambda=m\pi/a$ and $\mu=n\pi/b$.

By substituting expression (27) into the governing Eqs. (24), multiplying each equation by the corresponding eigenfunction, and integrating over the solution domain, the following equations are obtained after some mathematical manipulations:

$$\left(\begin{bmatrix}a_{11}&a_{12}&a_{13}&a_{14}\\a_{12}&a_{22}&a_{23}&a_{24}\\a_{13}&a_{23}&a_{33}&a_{34}\\a_{14}&a_{24}&a_{34}&a_{44}\end{bmatrix}-\omega^2\begin{bmatrix}m_{11}&0&m_{13}&m_{14}\\0&m_{22}&m_{23}&m_{24}\\m_{31}&m_{32}&m_{33}&m_{34}\\m_{41}&m_{42}&m_{43}&m_{44}\end{bmatrix}\right)\begin{Bmatrix}U_{mn}\\V_{mn}\\W_{mn}\\X_{mn}\end{Bmatrix}=\begin{Bmatrix}0\\0\\0\\0\end{Bmatrix} \tag{27}$$

in which

Table 1 The admissible functions for different boundary conditions Sobhy (2013)

Boundary Conditions	$x=0$	$y=0$	$x=a$	$y=b$	$X_m(x)$	$Y_n(y)$
SSSS	S	S	S	S	$sin(\lambda x)$	$sin(\mu x)$
CSCS	C	S	C	S	$sin^2(\lambda x)$	$sin(\mu x)$
CCCC	C	C	C	C	$sin^2(\lambda x)$	$sin^2(\mu x)$
FCFC	F	C	F	C	$cos^2(\lambda x)\,[sin^2(\lambda x)+1]$	$sin^2(\mu x)$

$$
\begin{aligned}
a_{11} &= A_{11}\alpha_{12} + A_{66}\alpha_8 \\
a_{12} &= (A_{12} + A_{66})\alpha_8 \\
a_{13} &= -B_{11}\alpha_{12} - (B_{12} + 2B_{66})\alpha_8 \\
a_{14} &= -(B^s_{12} + 2B^s_{66})\alpha_8 - B^s_{11}\alpha_{12} \\
a_{21} &= (A_{12} + A_{66})\alpha_{10} \\
a_{22} &= A_{22}\alpha_4 + A_{66}\alpha_{10} \\
a_{23} &= -B_{22}\alpha_4 - (B_{12} + 2B_{66})\alpha_{10} \\
a_{24} &= -(B^s_{12} + 2B_{66})\alpha_{10} - B^s_{22}\alpha_4 \\
a_{31} &= B_{11}\alpha_{13} + (B_{12} + 2B_{66})\alpha_{11} \\
a_{32} &= (B_{12} + 2B_{66})\alpha_{11} + B_{22}\alpha_5 \\
a_{33} &= -D_{11}\alpha_{13} - 2(D_{12} + 2D_{66})\alpha_{11} - D_{22}\alpha_5 \\
a_{34} &= -D^s_{11}\alpha_{13} - 2(D^s_{12} + 2D^s_{66})\alpha_{11} - D^s_{66}\alpha_5 \\
a_{41} &= B^s_{11}\alpha_{13} + (B^s_{12} + 2B^s_{66})\alpha_{11} \\
a_{42} &= (B^s_{12} + 2B^s_{66})\alpha_{11} + B^s_{22}\alpha_5 \\
a_{43} &= -D^s_{11}\alpha_{13} - 2(D^s_{12} + 2D^s_{66})\alpha_{11} - D^s_{22}\alpha_5 \\
a_{44} &= -H^s_{11}\alpha_{13} - 2(H^s_{12} + 2H^s_{66})\alpha_{11} - H^s_{22}\alpha_5 + A^s_{44}\alpha_9 + A^s_{55}\alpha_3
\end{aligned}
\tag{29a}
$$

$$
\begin{aligned}
m_{11} &= -I_0\alpha_6 \\
m_{13} &= -I_1\alpha_6 \\
m_{32} &= -I_1\alpha_3 \\
m_{14} &= J_1\alpha_6 \\
m_{33} &= -I_0\alpha_1 + I_2(\alpha_3 + \alpha_9) \\
m_{22} &= -I_0\alpha_2 \\
m_{34} &= -I_0\alpha_1 + J_2(\alpha_3 + \alpha_9) \\
m_{23} &= I_1\alpha_2 \quad , \quad m_{41} = -J_1\alpha_9
\end{aligned}
\tag{29b}
$$

$$m_{24} = J_1\alpha_2 \quad , \quad m_{42} = -J_1\alpha_3$$

$$m_{31} = -I_1\alpha_9 \quad , \; m_{44} = -I_0\alpha_1 + K_2(\alpha_3 + \alpha_9)$$

$$(\alpha_1, \alpha_3, \alpha_5) = \int_0^b \int_0^a (X_m Y_n, X_m Y_n'', X_m Y_n'''') \, X_m Y_n dxdy$$

$$(\alpha_2, \alpha_4, \alpha_{10}) = \int_0^b \int_0^a (X_m Y_n', X_m Y_n'', X_m'' Y_n') \, X_m Y_n' dxdy$$

$$(\alpha_6, \alpha_8, \alpha_{12}) = \int_0^b \int_0^a (X_m' Y_n, X_m' Y_n'', X_m''' Y_n) \, X_m' Y_n dxdy$$

$$(\alpha_7, \alpha_9, \alpha_{11}, \alpha_{13}) = \int_0^b \int_0^a (X_m' Y_n', X_m'' Y_n, X_m' Y_n'', X_m'''' Y_n) \, X_m Y_n dxdy$$

The nontrivial solution is obtained when the determinant of equation (25) equals zero.

4. Numerical Results and discussion

4.1 Validation

In this study, the free vibration of FG plates using the present refined plate theory was studied. The FG plate is taken to be made of aluminum (Al) and alumina (Al_2O_3) with the following material properties:

Ceramic (Alumina, Al2O3):$E_c = 380GPa, \; \nu = 0.3, \; \rho_c = 3800kg/m^3$.

Metal (Aluminum, Al):$E_m = 70GPa, \; \nu = 0.3, \; \rho_m = 2707kg/m^3$.

Numerical results are presented in terms of non-dimensional frequency. The non-dimensional parameter used is:

$$\hat{\omega} = \omega h \sqrt{\frac{\rho_c}{E_c}}$$

$$\overline{\omega} = \frac{\omega a^2}{h} \sqrt{\frac{\rho_c}{E_c}} \tag{30}$$

Table 2 highlights how material gradation, and thickness-to-length ratio (a/h) on the dynamic response of FG sandwich plates. The results confirm the accuracy of the present approach in predicting frequency behavior, making it a useful tool for structural analysis. The variation in fundamental frequency due to changes in material and geometry parameters was seen. A power-law FG materials (P-FGM) were considered and the grading index (p) was changed to 0, 0.5, 1, 4, and 10. The results are evaluated for multiple grading parameters and compared against established theoretical models.

The results are also presented for various vibration modes (***m***,***n***) of functionally graded plates under different power law indices (p). The results are compared using multiple higher-order and shear deformation theories, including Quasi-3D, Third-Order Shear Deformation Theory (TSDT),

Table 2 Comparison of the nondimensional frequencies $\hat{\omega}$ of simply supported Al/Al_2O_3 square plates

a/h	Mode (m,n)	Theory	Power law index (p)				
			0	0.5	1	4	10
5	1(1,1)	Quasi-3D Matsunaga (2008)	0.2121	0.1819	0.1640	0.1383	0.1306
		TSDT (Hosseini-Hashemi *et al*. (2011)	0.2113	0.1807	0.1631	0.1378	0.1301
		FSDT (Hosseini-Hashemi *et al*. (2011)	0.2112	0.1805	0.1631	0.1397	0.1324
		HSDT Thai and Kim (2013)	0.2113	0.1807	0.1631	0.1378	0.1301
		Nguyen (2015)	0.2117	0.1810	0.1634	0.1378	0.1303
		Present	0.2112	0.1807	0.1631	0.1377	0.1300
	2(1,2)	Quasi-3D Matsunaga (2008)	0.4658	0.4040	0.3644	0.3000	0.2790
		TSDT (Hosseini-Hashemi *et al*. (2011)	0.4623	0.3989	0.3607	0.2980	0.2771
		FSDT (Hosseini-Hashemi *et al*. (2011)	0.4618	0.3978	0.3604	0.3049	0.2856
		HSDT Thai and Kim (2013)	0.4623	0.3989	0.3607	0.2980	0.2771
		Nguyen (2015)	0.4645	0.4004	0.3622	0.2931	0.2783
		Present	0.4624	0.3990	0.3608	0.2977	0.2770
	3(2,2)	TSDT (Hosseini-Hashemi *et al*. (2011)	0.6688	0.5803	0.5254	0.4284	0.3948
		FSDT (Hosseini-Hashemi *et al*. (2011)	0.6676	0.5779	0.5245	0.4405	0.4097
		HSDT Thai and Kim (2013)	0.6688	0.5803	0.5254	0.4284	0.3948
		Nguyen (2015)	0.6734	0.5836	0.5286	0.4291	0.3974
		Present	0.6693	0.5806	0.5257	0.4280	0.3948
10	1(1,1)	Quasi-3D Matsunaga (2008)	0.0578	0.0492	0.0443	0.0381	0.0364
		TSD (Hosseini-Hashemi *et al*. (2011)	0.0577	0.0490	0.0442	0.0381	0.0364
		FSDT (Hosseini-Hashemi *et al*. (2011)	0.0577	0.0490	0.0442	0.0382	0.0364
		HSDT Thai and Kim (2013)	0.0577	0.0490	0.0442	0.0381	0.0364
		Nguyen (2015)	0.0577	0.0490	0.0442	0.0381	0.0364
		Present	0.0576	0.0490	0.0441	0.0380	0.0363
	2(1,2)	Quasi-3D Matsunaga (2008)	0.1381	0.1180	0.1063	0.0905	0.0859
		TSDT (Hosseini-Hashemi *et al*. (2011)	0.1377	0.1174	0.1059	0.0903	0.0856
		FSDT (Hosseini-Hashemi *et al*. (2011)	0.1376	0.1173	0.1059	0.0911	0.0867
		HSDT Thai and Kim (2013)	0.1377	0.1174	0.1059	0.0903	0.0856
		Nguyen (2015)	0.1379	0.1175	0.1060	0.0902	0.0857
		Present	0.1376	0.1173	0.1059	0.0902	0.0856
	3(2,2)	TSDT (Hosseini-Hashemi *et al*. (2011)	0.2113	0.1807	0.1631	0.1378	0.1301
		FSDT (Hosseini-Hashemi *et al*. (2011)	0.2112	0.1805	0.1631	0.1378	0.1301
		HSDT Thai and Kim (2013)	0.2113	0.1807	0.1631	0.1378	0.1301
		Nguyen (2015)	0.2117	0.1810	0.1634	0.1378	0.1301
		Present	0.2112	0.1807	0.1631	0.1377	0.1300
20	1(1,1)	TSDT (Hosseini-Hashemi *et al*. (2011)	0.0148	0.0125	0.0113	0.0098	0.0094
		FSDT (Hosseini-Hashemi *et al*. (2011)	0.0148	0.0125	0.0113	0.0098	0.0094
		HSDT Thai and Kim (2013)	0.0148	0.0125	0.0113	0.0098	0.0094

	Nguyen (2015)	0.0148	0.0125	0.0113	0.0098	0.0094
	Present	0.0148	0.0125	0.0113	0.0098	0.0094
2(1,2)	Nguyen (2015)	0.0365	0.0310	0.0279	0.0241	0.0231
	Present	0.0365	0.0310	0.0279	0.0241	0.0231
3(2,2)	Nguyen (2015)	0.0577	0.0490	0.0442	0.0381	0.0364
	Present	0.0577	0.0490	0.0442	0.0380	0.0363

First-Order Shear Deformation Theory (FSDT), and Higher-Order Shear Deformation Theory (HSDT). The minor difference seen is because of variations in modeling assumptions and numerical techniques.

Table 3 illustrates the influence of the power law index (***p***) and geometry parameter (***a/b*** and ***a/h***) on the fundamental frequency of functionally graded (FG) plates. As the grading parameter increases, a notable shift in natural frequencies is observed, reflecting the gradual transition from a ceramic-rich composition to a metal-rich composition. The results indicate that a higher grading parameter reduces the stiffness of the structure, leading to decreased natural frequencies. Furthermore, the comparison with existing studies confirms the accuracy of the present approach. It should be noted that increasing the geometry parameters (***a/b*** and ***a/h***) increases the natural frequency.

4.2 Effect of micromechanical models on free vibration analysis of FG plates

The effect of micromechanical models on free vibration analysis of FG plates under various boundary conditions using the present trigonometric shear deformation plate theory (TSDPT) is presented for investigation. The results are presented in Tables 4-7 for the FG plate with different values of power law index p and two values of a/h.

Table 4 presents the natural frequency results of SSSS FG plates for different micromechanical models, a***/h*** values, and material gradations. The grading parameter varies from 0, 0.5, 1, 2, and 5, while ***a/h*** values are varied from 5 and 10. The higher the grading indices, the lower the natural frequency will be. The different well-known micromechanical models chosen are Voigt, Reuss, LRVE, Tamura, and Mori-Tanaka. Of these, the Voigt model, which describes the upper bound, yields the maximum frequency, while Reuss, which gives the lower bound, yields the lowest. LRVE and Mori-Tanaka models provide intermediate values, reflecting a balance between strain and stress considerations.

Table 5 illustrates the results for the CCCC plate, in the Voigt model, the fundamental frequency for ***p*** = 0 drops from 0.3505 to 0.1041, a 70.32% decrease. When ***p***=0.5, compared to Voigt, Reuss gives (20.47 % lower than Voigt), LRVE (13.25% lower), Tamura (q=0) (18.71% lower), Tamura (q=100 (11.58% lower), Mori-Tanaka: 2533 (16.49% lower). However, when p=5, Reuss (6.79% lower), LRVE (5.98% lower), Tamura (q=0) (8.15% lower), Tamura (q=100) (5.79% lower), Mori-Tanaka (8.08% lower). It is interesting to note that as the grading indices values are higher, the micromechanical models have an insignificant impact on the natural frequency.

For the CSCS FG plate, the fundamental frequency in the Voigt model declines from 0.2939 at p = 0 to 0.1865 at ***p***=5, a 36.52% decrease, please see Table 6. When comparing micromechanical models at p=0.5, the Reuss model predicts a 20.24% lower frequency than Voigt, while LRVE, Tamura (q=0), Tamura (***q***=100), and Mori-Tanaka models show 13.29 %, 18.15 %, 11.92 %, and

Table 3 Nondimensional natural frequencies $\overline{\omega}$ of simply supported Al/Al_2O_3 square plates.

a/b	a/h	Mode (m,n)	Theory	Power law index (p)					
				0	0.5	1	2	5	10
0.5	5	1(1,1)	Nguyen (2015)	3.4464	2.9380	2.6509	2.3971	2.2260	2.1432
			Present	3.4416	2.9348	2.6477	2.3947	2.2260	2.1403
		2(1,2)	Nguyen (2015)	5.2932	4.5258	4.0860	3.6859	3.3919	3.2574
			Present	5.2822	4.5186	4.0786	3.6804	3.3913	3.2506
		3(2,2)	Nguyen (2015)	11.6113	10.0109	9.0538	8.1181	7.2951	6.9568
			Present	11.5614	9.9754	9.0200	8.0914	7.2869	6.9259
	10	1(1,1)	Nguyen (2015)	3.6533	3.0996	2.7946	2.5371	2.3911	2.3118
			Present	3.6518	3.0990	2.7937	2.5364	2.3912	2.3108
		2(1,2)	Nguyen (2015)	5.7731	4.9031	4.4216	4.0105	3.7671	3.6388
			Present	5.7696	4.9016	4.4190	4.0088	3.7672	3.6364
		3(2,2)	Nguyen (2015)	13.7855	11.7519	10.6036	9.5884	8.9042	8.5729
			Present	13.7664	11.7398	10.5910	9.5791	8.9034	8.5611
	20	1(1,1)	Nguyen (2015)	3.7127	3.1455	2.8355	2.5773	2.4401	2.3622
			Present	3.7123	3.1458	2.8352	2.5771	2.4401	2.3618
		2(1,2)	Nguyen (2015)	5.9309	5.0176	4.5234	4.1104	3.8880	3.7629
			Present	5.9199	5.0180	4.5228	4.1100	3.8880	3.7621
		3(2,2)	Nguyen (2015)	14.6131	12.3983	11.1784	10.1482	9.5645	9.2471
			Present	14.6075	12.3963	11.1749	10.1456	9.5648	9.2433
1	5	1(1,1)	Nguyen (2015)	5.2932	4.5258	4.0860	3.6859	3.3919	3.2574
			Present	5.2822	4.5186	4.0786	3.6804	3.3913	3.2506
		2(1,2)	Nguyen (2015)	11.6113	10.0109	9.0538	8.1181	7.2951	6.9568
			Present	11.5614	9.9754	9.0200	8.0914	7.2869	6.9259
		3(2,2)	Nguyen (2015)	16.8351	14.5888	13.2140	11.8101	10.4647	9.9360
			Present	16.7328	14.5155	13.1438	11.7527	10.4400	9.8710
	10	1(1,1)	Nguyen (2015)	5.7731	4.9031	4.4216	4.0105	3.7671	3.6388
			Present	5.7696	4.9016	4.8194	4.0088	3.7673	3.6364
		2(1,2)	Nguyen (2015)	13.7855	11.7519	10.6036	9.5884	8.9042	8.5729
			Present	13.7664	11.7398	10.5911	9.5791	8.9004	8.5611
		3(2,2)	Nguyen (2015)	21.1728	18.1033	16.3438	14.7435	13.5677	13.0296
			Present	21.1288	18.0746	16.3147	14.7217	13.5655	13.0024
	20	1(1,1)	Nguyen (2015)	5.9209	5.0176	4.5234	4.1104	3.8880	3.7629
			Present	5.9200	5.0180	4.5228	4.1100	3.8880	3.7621
		2(1,2)	Nguyen (2015)	14.6131	12.3983	11.1784	10.1482	9.5645	9.2471
			Present	14.6075	12.3963	11.1749	10.1456	9.5648	9.2433
		3(2,2)	Nguyen (2015)	23.0925	19.6126	17.6865	16.0419	15.0685	14.5550
			Present	23.0786	19.6065	17.6778	16.0364	15.0690	14.5458

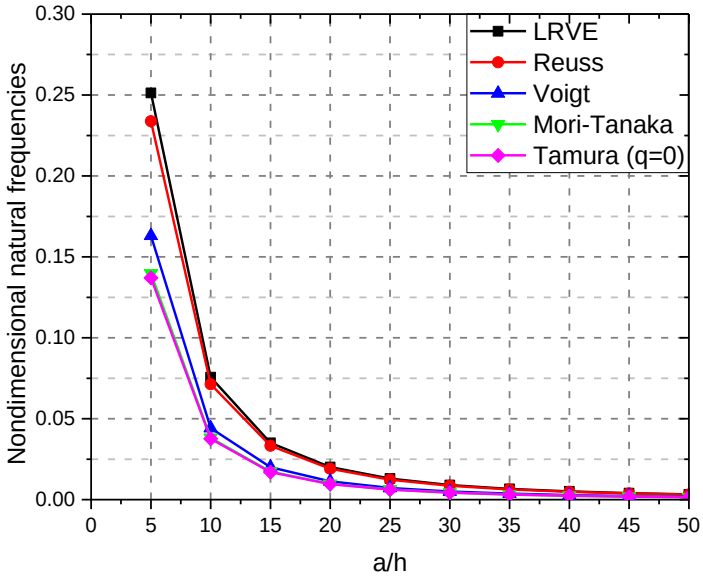

Fig. 2 Variation of the nondimensional frequencies through the thickness for simply supported FGM plate for different micromechanical models (p=1)

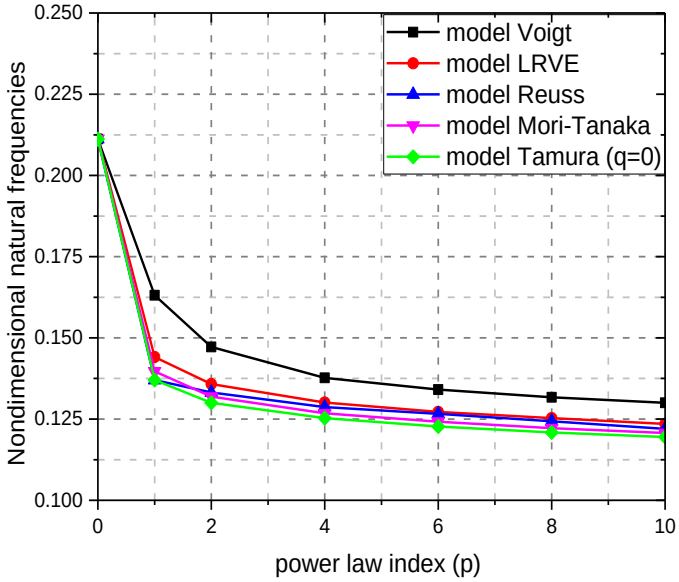

Fig. 3 Nondimensional frequencies $\hat{\omega}$ verss the power law index p for simply supported of FG plates for different micromechanical models (a/h=5)

16.31 % lower values, respectively. At p = 5, the differences narrow, with Reuss predicting 6.64% lower than Voigt, LRVE 5.75 % lower, Tamura (q = 0) 9.00 % lower, Tamura (q = 100) 5.61 % lower, and Mori-Tanaka 7.86 % lower. Moreover, increasing a/h from 5 to 10 results in a

Table 4 Variation of the fundamental frequency $\overline{\omega}$ with the power-law index p for SSSS FG plate

a/h	Model		Power law index (p)				
			0	0.5	1	2	5
5		Voigt	0.2112	0.1807	0.1631	0.1472	0.1356
		Reuss	0.2112	0.1447	0.1370	0.1332	0.1270
		LRVE	0.2112	0.1592	0.1454	0.1358	0.1285
	Tamura	q=0	0.2112	0.1479	0.1370	0.1300	0.1239
		q=100	0.2112	0.1601	0.1460	0.1362	0.1285
	Mori-Tanaka		0.2112	0.1516	0.1397	0.1319	0.1253
10		Voigt	0.0576	0.0490	0.0442	0.0400	0.0376
		Reuss	0.0576	0.0394	0.0376	0.0368	0.0353
		LRVE	0.0576	0.0434	0.0396	0.0374	0.0358
	Tamura	q=0	0.0576	0.0403	0.0376	0.0359	0.0344
		q=100	0.0576	0.0435	0.0398	0.0374	0.0357
	Mori-Tanaka		0.0576	0.0413	0.0382	0.0364	0.0348

Table 5 Variation of fundamental frequency $\overline{\omega}$ with the power-law index p for CCCC FG plate

a/h	Model		Power law index (p)				
			0	0.5	1	2	5
5		Voigt	0.3505	0.3033	0.2747	0.2466	0.2208
		Reuss	0.3505	0.2413	0.2267	0.2177	0.2058
		LRVE	0.3505	0.2631	0.2430	0.2236	0.2076
	Tamura	0.3505	0.2465	0.2267	0.2126	0.2028	0.1239
		0.3505	0.2682	0.2437	0.2244	0.2080	0.1285
	Mori-Tanaka		0.3505	0.2533	0.2318	0.2161	0.2030
10		Voigt	0.1041	0.0889	0.0802	0.0726	0.0674
		Reuss	0.1041	0.0714	0.0677	0.0660	0.0630
		LRVE	0.1041	0.0783	0.0717	0.0673	0.0639
	Tamura	0.1041	0.0729	0.0677	0.0644	0.0615	0.0344
		0.1041	0.0788	0.0720	0.0674	0.0638	0.0357
	Mori-Tanaka		0.1041	0.0747	0.0690	0.0654	0.0622

frequency reduction of 71.29 %, highlighting the effect of increasing thickness on lowering fundamental frequencies.

For the FCFC FG plate as shown in Table 7, the fundamental frequency in the Voigt model reduces from 0.3617 at p = 0 to 0.2266 at p = 5, marking a 37.35% decrease. At p = 0.5, the Reuss model predicts a 20.41 % lower frequency than Voigt, while LRVE, Tamura (q = 0), Tamura (q = 100), and Mori-Tanaka models predict 13.47 %, 18.71 %, 11.56 %, and 16.69 % lower values, respectively. At p = 5, the differences among models become smaller, with Reuss predicting 6.68% lower than Voigt, LRVE 5.97% lower, Tamura (q = 0) 8.92% lower, Tamura (q = 100) 5.82% lower, and Mori-Tanaka 7.99% lower. Additionally, increasing a/h from 5 to 10 leads to a 69.66%

Table 6 Variation of fundamental frequency $\overline{\omega}$ with the power-law index p for CSCS FG plate

a/h	Model		Power law index (p)				
			0	0.5	1	2	5
5		Voigt	0.2939	0.2532	0.2291	0.2060	0.1865
		Reuss	0.2939	0.2020	0.1903	0.1836	0.1741
		LRVE	0.2939	0.2195	0.2032	0.1881	0.1758
	Tamura	0.2939	0.2064	0.1903	0.1793	0.1699	0.1239
		0.2939	0.2241	0.2039	0.1887	0.1760	0.1285
	Mori-Tanaka		0.2939	0.2118	0.1944	0.1821	0.1718
10		Voigt	0.0844	0.0719	0.0649	0.0588	0.0548
		Reuss	0.0844	0.0518	0.0549	0.0537	0.0513
		LRVE	0.0844	0.0637	0.0581	0.0546	0.0520
	Tamura	0.0844	0.0591	0.0549	0.0524	0.0500	0.0344
		0.0844	0.0638	0.0583	0.0547	0.0520	0.0357
	Mori-Tanaka		0.0844	0.0605	0.0560	0.0531	0.0507

Table 7 Variation of fundamental frequency $\overline{\omega}$ with the power-law index p for FCFC FG plate

a/h5	Model		Power law index (p)				
			0	0.5	1	2	5
5		Voigt	0.3617	0.3139	0.2847	0.2552	0.2266
		Reuss	0.3617	0.2494	0.2338	0.2239	0.2113
		LRVE	0.3617	0.2766	0.2513	0.2304	0.2130
	Tamura	0.3617	0.2548	0.2338	0.2186	0.2061	0.1239
		0.3617	0.2775	0.2519	0.2312	0.2134	0.1285
	Mori-Tanaka		0.3617	0.2618	0.2393	0.2224	0.2084
10		Voigt	0.1097	0.0937	0.0847	0.0765	0.7083
		Reuss	0.1097	0.0752	0.0713	0.0694	0.0662
		LRVE	0.1097	0.0830	0.0756	0.0708	0.0671
	Tamura	0.1097	0.0768	0.0713	0.0678	0.0646	0.0344
		0.1097	0.0831	0.0759	0.0709	0.0670	0.0357
	Mori-Tanaka		0.1097	0.0788	0.0727	0.0687	0.0654

frequency drop, reaffirming that the plate's stiffness decreases with a higher aspect ratio.

Fig. 2 illustrates the non-dimensional frequency results with various a/h values. The LRVE model yields maximum frequency followed by Reuss, Voigt, Mori-Tanaka, and Tamura. It should be noted that when the magnitude of ***a/h*** is higher, here (for ***a/h***>20) the models LRVE, Reuss and Mori-Tanaka, and Voigt give similar results. Also, beyond a certain value of a/h the variation in natural frequency becomes constant, up to ***a/h***>15, the drop is steeper.

Similarly, the grading indices are plotted with natural frequency as shown in Figure 3. For lower grading indices (***p***<4) there is a drastic change in natural frequency was seen, however, as the indices are increased further, the variation becomes constant.

5. Conclusions

Free vibration problems were solved using Hamilton's principle and Navier's procedure, analyzing the effects of various boundary conditions, micromechanical models, and key geometrical parameters. The following are the conclusions from the study:

1. The fundamental frequency decreases as the power-law index increases from 0 to 5 for all models. Because of changes in the overall composition from ceramic-rich to metal-rich.

2. The Mori-Tanaka and LRVE models offer a more realistic prediction for practical applications, as they account for both matrix and reinforcement interactions. The Voigt and Reuss models yield the upper and lower bound values and so can be used to develop and test novel micromechanical models.

3. The CCCC (Clamped-Clamped) plates exhibit the highest fundamental frequencies due to the fully constrained edges. The SSSS (Simply Supported) shows the lowest natural frequency while FCFC and CSCS show intermediate results.

4. A higher aspect ratio (***a/h***) results in significantly reduced fundamental frequency values. Lower range variation of geometry parameters and grading parameters has a higher impact than the higher range of values of these ratios.

5. The results emphasize the need to choose an appropriate homogenization model depending on the specific application, especially in cases where microstructural effects significantly influence the material behavior.

References

Addou, F.Y., Meradjah, M., Bousahla, A.A., Benachour, A., Bourada, F., Tounsi, A. and Mahmoud, S.R. (2019), "Influences of porosity on dynamic response of FG plates resting on Winkler/Pasternak/Kerr foundation using quasi 3D HSDT", *Comput. Concr.*, **24**(4), 347-367. https://doi.org/10.12989/CAC.2019.24.4.347

Affdl, J.C.H. and Kardos, J.L. (1976), "The Halpin-Tsai equations: A review" *Polym. Eng. Sci.*, **16**(5), 344-352. https://doi.org/10.1002/pen.760160512

Akbarzadeh, A.H., Abedini, A. and Chen, Z.T. (2015), "Effect of micromechanical models on structural responses of functionally graded plates", *Compos. Struct.*, **119**, 598-609. https://doi.org/10.1016/j.compstruct.2014.09.031

Ali, M.I. and Azam, M.S. (2021), "Exact solution by dynamic stiffness method for the natural vibration of porous functionally graded plate considering neutral surface", *Proceedings of the Institution of Mechanical Engineers*, *Part L: Journal of Materials: Design and Applications*, **235**(7), 1585-1603. https://doi.org/10.1177/1464420720988170

Alibeigloo, A. and Liew, K.M. (2014), "Free vibration analysis of sandwich cylindrical panel with functionally graded core using three-dimensional theory of elasticity", *Compos. Struct.*, **113**, 23-30. https://doi.org/10.1016/j.compstruct.2014.03.004

Allam, M.N.M., Tantawy, R. and Zenkour, A.M. (2018), "Magneto-thermo-elastic response of exponentially graded piezoelectric hollow spheres", *Adv. Comput. Des.*, **3**(3), 303-318. https://doi.org/10.12989/ACD.2018.3.3.303

Almasi, D., Sadeghi, M., Lau, W.J., Roozbahani, F. and Iqbal, N. (2016), "Functionally graded polymeric materials: A brif review of current fabrication methods and introduction of a novel fabrication method", *Mater. Sci. Eng. C*, **64**, 102-107. https://doi.org/10.1016/j.msec.2016.03.053

Alnujaie, A., Ghazwani, M.H., Assie, A.E., Eltaher, M.A. and Van Vinh, P. (2025), "Damped vibration characteristics of functionally graded sandwich beams resting on an advanced viscoelastic foundation

model", *Acta Mech*., 2025. https://doi.org/10.1007/s00707-025-04439-x
Altabey, W.A. (2017), "A study on thermo-mechanical behavior of MCD through bulge test analysis", *Adv*. *Comput*. *Des*., **2**(2), 107-119. https://doi.org/10.12989/ACD.2017.2.2.107
Arefi, M., Mohammad-Rezaei Bidgoli, E., Dimitri, R. and Tornabene, F. (2018), "Free vibrations of functionally graded polymer composite nanoplates reinforced with graphene nanoplatelets", *Aerosp*. *Sci*. *Technol*., **81**, 108-117. https://doi.org/10.1016/j.ast.2018.07.036
Bakar, W.Z.W., Basri, S., Jamaludin, S.N.S. and Sajjad, A. (2018), "Functionally graded materials: An overview of dental applications", *World J*. *Dent*., **9**(2), 137-144. https://doi.org/10.5005/jp-journals-10015-1523
Balubaid, M., Tounsi, A., Dakhel, B. and Mahmoud, S.R. (2019), "Free vibration investigation of FG nanoscale plate using nonlocal two variables integral refined plate theory", *Comput*. *Concr*., **24**(6), 579-586. https://doi.org/10.12989/CAC.2019.24.6.579
Bayat, M., Saleem, M., Sahari, B.B., Hamouda, A.M.S. and Mahdi, E. (2008), "Analysis of functionally graded rotating disks with variable thickness", *Mech*. *Res*. *Commun*., **35**(5), 283-309. https://doi.org/10.1016/j.mechrescom.2008.02.007
Bendenia, N., Zidour, M., Bousahla, A.A., Bourada, F., Tounsi, A., Benrahou, K.H., Bedia, E.A.A., Mahmoud, S.R. and Tounsi, A. (2020), "Deflections, stresses and free vibration studies of FG-CNT reinforced sandwich plates resting on Pasternak elastic foundation", *Comput*. *Concr*., **26**(3), 213-226. https://doi.org/10.12989/CAC.2020.26.3.213
Benveniste, Y. (1987), "A new approach to the application of Mori-Tanaka's theory in composite materials", *Mech*. *Mater*., **6**(2), 147-157. https://doi.org/10.1016/0167-6636(87)90005-6
Birman, V. and Kardomateas, G.A. (2018), "Review of current trends in research and applications of sandwich structures", *Compos*. *Part B Eng*., **142**, 221-240. https://doi.org/10.1016/j.compositesb.2018.01.027
Blanco, P.J., Sánchez, P.J., de Souza Neto, E.A. and Feijóo, R.A. (2016), "Variational foundations and generalized unified theory of rve-based multiscale models", *Arch*. *Comput*. *Methods Eng*., **23**(2), 191-253. https://doi.org/10.1007/s11831-014-9137-5
Djilali Djebbour, K., Mokhtar, N., Hassen, A.A., Alghanmi, R.A., Hadji, L. and Riadh, B. (2024), "An enhanced quasi-3D HSDT for free vibration analysis of porous FG-CNT beams on a new concept of orthotropic VE-foundations", *Mech*. *Adv*. *Mater*. *Struct*., **32**(5), 893-909. https://doi.org/10.1080/15376494.2024.2356728
Duc, N.D., Bich, D.H. and Cong, P.H. (2016), "Nonlinear thermal dynamic response of shear deformable FGM plates on elastic foundations", *J*. *Therm*. *Stress*., **39**(3), 278-297. https://doi.org/10.1080/01495739.2015.1125194
Ermakova, A., Mehmanparast, A. and Ganguly, S. (2019), "A review of present status and challenges of using additive manufacturing technology for offshore wind applications", *Procedia Struct*. *Integr*., **17**, 29-36. https://doi.org/10.1016/j.prostr.2019.08.005
Gao, K., Gao, W., Chen, D. and Yang, J. (2018), "Nonlinear free vibration of functionally graded graphene platelets reinforced porous nanocomposite plates resting on elastic foundation", *Compos*. *Struct*., **204**, 831-846. https://doi.org/10.1016/j.compstruct.2018.08.013
Ghazwani, M.H., Alnujaie, A., Avcar, M., Van Vinh, P. (2024), "Examination of the high-frequency behavior of functionally graded porous nanobeams using nonlocal simple higher-order shear deformation theory", *Acta Mech*., **235**, 2695-2714. https://doi.org/10.1007/s00707-024-03858-6
Hadji, L., Zouatnia, N. and Bernard, F. (2019), "An analytical solution for bending and free vibration responses of functionally graded beams with porosities: Effect of the micromechanical models", *Struct*. *Eng*. *Mech*., **69**(2), 231-241. https://doi.org/10.12989/sem.2019.69.2.231
Hadji, L., Plevris, V., Madan, R. (2025), "Dynamic behavior of imperfect FGM beams with various porosity distribution rates: analysis and modeling". *In: Kioumarsi*, *M*., *Shafei*, *B*. *(eds) The 1st International Conference on Net-Zero Built Environment*, *NTZR 2024*, *Lecture Notes in Civil Engineering*, **237**. Springer, Cham. https://doi.org/10.1007/978-3-031-69626-8_126
Kapuria, S., Bhattacharyya, M. and Kumar, A.N. (2008), "Theoretical modeling and experimental validation

of thermal response of metal-ceramic functionally graded beams", *J. Therm. Stress.*, **31**(8), 759-787. https://doi.org/10.1080/01495730802194292

Karamanlı, A. (2018), "Free vibration analysis of two directional functionally graded beams using a third order shear deformation theory", *Compos. Struct.*, **189**, 127-136. https://doi.org/10.1016/j.compstruct.2018.01.060

Kim, Y.W. (2015), "Free vibration analysis of FGM cylindrical shell partially resting on Pasternak elastic foundation with an oblique edge", *Compos. Part B Eng.*, **70**, 263-276. https://doi.org/10.1016/j.compositesb.2014.11.024

Kitipornchai, S., Yang, J. and Liew, K.M. (2006), "Random vibration of the functionally graded laminates in thermal environments", *Comput. Method Appl. Mech. Eng.*, **195**(9), 1075-1095. https://doi.org/10.1016/j.cma.2005.01.016

Lal, A., Jagtap, K.R. and Singh, B.N. (2017), "Thermo-mechanically induced finite element based nonlinear static response of elastically supported functionally graded plate with random system properties", *Adv. Comput. Des.*, **2**(3), 165-194. https://doi.org/10.12989/ACD.2017.2.3.165

Lakel, A., Hadji, L., Avcar, M., Ait Atmane, H., and Madan, R. (2024). "The natural frequency analysis of FG-GNPR nanoplates under different boundary conditions", *Adv. Nano Res.*, **17**(6), 533-546. https://doi.org/10.12989/anr.2024.17.6.533

Lang, Z. and Xuewu, L. (2013), "Buckling and vibration analysis of functionally graded magneto-electro-thermo-elastic circular cylindrical shells", *Appl. Math. Modell.*, **37**(4), 2279-2292. https://doi.org/10.1016/j.apm.2012.05.023

Madan, R. and Bhowmick, S. (2021), "Modeling of functionally graded materials to estimate effective thermo-mechanical properties", *World J. Eng.*, **19**(3), 291-301. https://doi.org/10.1108/WJE-09-2020-0445

Madan, R., Bhowmick, S. and Saha, K. (2020), "A study based on stress-strain transfer ratio calculation using Halpin-Tsai and MROM material model for limit elastic analysis of metal matrix FG rotating disk", *FME Transact.*, **48**(2), 204-210. https://doi.org/10.5937/fmet2001204R

Madan, R., Khobragade, P., Mussada, E.K., Singh, M.K., Rangappa, S.M., Njim, E.K. and Siengchin, S. (2025), "A novel two-step finite element approach to estimate the thermo-mechanical properties of two-phase and three-phase hybrid composites", *Compos. Commun.*, **53**, 102213. https://doi.org/10.1016/j.coco.2024.102213

Mechab, B., Mechab, I., Benaissa, S., Ameri, M. and Serier, B. (2016), "Probabilistic analysis of effect of the porosities in functionally graded material nanoplate resting on Winkler-Pasternak elastic foundations", *Appl. Math. Modell.*, **40**(2), 738-749. https://doi.org/10.1016/j.apm.2015.09.093

Nakamura, T., Wang, T. and Sampath, S. (2000), "Determination of properties of graded materials by inverse analysis and instrumented indentation", *Acta Materialia*, **48**(17), 4293-4306. https://doi.org/10.1016/S1359-6454(00)00217-2

Nebab, M., Dahmane, M., Belqassim, A., Atmane, H. A., Bernard, F., Benadouda, M., Hadji, L. (2023). "Fundamental frequencies of cracked FGM beams with influence of porosity and Winkler/Pasternak/Kerr foundation support using a new quasi-3D HSDT", *Mech. Adv. Mater. Struct.*, **31**(28), 10639-10651. https://doi.org/10.1080/15376494.2023.2294371

Nie, G.J. and Zhong, Z. (2007), "Semi-analytical solution for three-dimensional vibration of functionally graded circular plates", *Comput. Methods Appl. Mech. Eng.*, **196**, 4901-4910. https://doi.org/10.1016/j.cma.2007.06.028

Qian, L.F., Batra, R.C. and Chen, L.M. (2003), "Free and forced vibrations of thick rectangular plates using higher-order shear and normal deformable plate theory and meshless Petrov-Galerkin (MLPG) method", *Comput. Model. Eng. Sci.*, **4**(5), 519-534. https://doi.org/10.3970/cmes.2003.004.519

Reuss, A. (1929), "Berechnung der Fließgrenze von Mischkristallen auf Grund der Plastizitätsbedingung für Einkristalle", *ZAMM Zeitschrift für Angewandte Mathematik und Mechanik*, **9**(1), 49-58. https://doi.org/10.1002/zamm.19290090104

Singh, A. and Kumari, P. (2020), "Analytical free vibration solution for angle-ply piezolaminated plate under cylindrical bending: A piezo-elasticity approach", *Adv. Comput. Des.*, **5**(1), 55-89.

https://doi.org/10.12989/ACD.2020.5.1.055
Srivastava, M.C., Singh, S., Rajak, B., Sharma, H.K., Kumar, R. and Singh, J. (2025), "Buckling response of two-directional skew FGM plate resting on elastic foundation: A RBFMC approach", *Comput. Concr.*, **35**(4), 357-367. https://doi.org/10.12989/cac.2025.35.4.357
Suresh, S. and Mortense,n, A. (1997), "Functionally graded metals and metal-ceramic composites: Part 2 Thermomechanical behaviour", *Int. Mater. Rev.*, **42**(3), 85-116. https://doi.org/10.1179/imr.1997.42.3.85
Thai, H.T. and Choi, D.H. (2014), "Levy solution for free vibration analysis of functionally graded plates based on a refined plate theory", *KSCE J. Civil Eng.*, **18**(6), 1813-1824. https://doi.org/10.1007/s12205-014-0409-2
Touratier, M. (1991), "An efficient standard plate theory", *Int. J. Eng. Sci.*, **29**(8), 901-916. https://doi.org/10.1016/0020-7225(91)90117-Y
Voigt, W. (1889), "Ueber die Beziehung zwischen den beiden Elasticitätsconstanten isotroper Körper", *Annalen der Physik*, **274**(12), 573-587. https://doi.org/10.1002/andp.18892741206
Wang, Y.X., Tang, Y. and Yang, T.Z. (2024), "Nonlinear mechanic analysis of a composite pipe conveying solid-liquid two-phase flow", *Appl. Ocean Res.*, **144**, 103905. https://doi.org/10.1016/j.apor.2024.103905
Yu, J. and Kidane, A. (2014), "Modeling functionally graded materials containing multiple heterogeneities", *Acta Mechanica*, **225**(7), 1931-1943. https://doi.org/10.1007/s00707-013-1033-9
Zenkour, A.M. and Abouelregal, A.E. (2018), "Decaying temperature and dynamic response of a thermoelastic nanobeam to a moving load", *Adv. Comput. Des.*, **3**(1), 1-16. https://doi.org/10.12989/ACD.2018.3.1.001
Zhao, J., Xie, F., Wang, A., Shuai, C., Tang, J. and Wang, Q. (2019), "Dynamics analysis of functionally graded porous (FGP) circular, annular and sector plates with general elastic restraints", *Compos. Part B Eng.*, **159**, 20-43. https://doi.org/10.1016/j.compositesb.2018.08.114
Zhu, P. and Liew, K.M. (2012), "A local Kriging meshless method for free vibration analysis of functionally graded circular plates in thermal environments", *Int. Conference Adv. Comput. Model. Simul.*, **31**, 1089-1094. https://doi.org/10.1016/j.proeng.2012.01.1147
Zouatnia, N., Hadji, L., Atmane, H.A., Nebab, M., Madan, R., Bennai, R. and Dahmane, M. (2024), "Analysis of free vibration in bi-directional power law-based FG beams employing RSD theory", *Coupled Syst. Mech.*, **13**(4), 359-373. https://doi.org/10.12989/CSM.2024.13.4.359

CC